THE JOURNAL OF BIOLOGICAL CHEMISTRY VOL. 281, NO. 11, pp. 7309–7316, March 17, 2006
Printed in the U.S.A.

Structural and Computational Analysis of the Quinone-binding Site of Complex II (Succinate-Ubiquinone Oxidoreductase)

*A MECHANISM OF ELECTRON TRANSFER AND PROTON CONDUCTION DURING UBIQUINONE REDUCTION**

Received for publication, July 26, 2005, and in revised form, November 9, 2005 Published, JBC Papers in Press, December 27, 2005, DOI 10.1074/jbc.M508173200

Rob Horsefield[‡1], Victoria Yankovskaya[§], Graham Sexton[¶], William Whittingham[¶], Kazuro Shiomi[‖], Satoshi Ōmura[**], Bernadette Byrne[‡], Gary Cecchini[§2], and So Iwata[‡3]

*From the [‡]Division of Molecular Biosciences, Imperial College London, London SW7 2AZ, United Kingdom, the [§]Molecular Biology Division, Department of Veterans Affairs Medical Center, San Francisco, California 94121, the Department of Biochemistry & Biophysics, University of California, San Francisco, California 94143, [¶]Syngenta, Jealott's Hill International Research Centre, Bracknell RG42 6EY, United Kingdom, [‖]The School of Pharmaceutical Sciences, Kitasato University, Minato-ku, Tokyo 108-8641, Japan, and the **Kitasato Institute, 9-1, Shirokane 5-chome, Minato-ku, Tokyo 108-8642, Japan*

The transfer of electrons and protons between membrane-bound respiratory complexes is facilitated by lipid-soluble redox-active quinone molecules (Q). This work presents a structural analysis of the quinone-binding site (Q-site) identified in succinate:ubiquinone oxidoreductase (SQR) from *Escherichia coli*. SQR, often referred to as Complex II or succinate dehydrogenase, is a functional member of the Krebs cycle and the aerobic respiratory chain and couples the oxidation of succinate to fumarate with the reduction of quinone to quinol (QH_2). The interaction between ubiquinone and the Q-site of the protein appears to be mediated solely by hydrogen bonding between the O1 carbonyl group of the quinone and the side chain of a conserved tyrosine residue. In this work, SQR was co-crystallized with the ubiquinone binding-site inhibitor Atpenin A5 (AA5) to confirm the binding position of the inhibitor and reveal additional structural details of the Q-site. The electron density for AA5 was located within the same hydrophobic pocket as ubiquinone at, however, a different position within the pocket. AA5 was bound deeper into the site prompting further assessment using protein-ligand docking experiments *in silico*. The initial interpretation of the Q-site was re-evaluated in the light of the new SQR-AA5 structure and protein-ligand docking data. Two binding positions, the Q_1-site and Q_2-site, are proposed for the *E. coli* SQR quinone-binding site to explain these data. At the Q_2-site, the side chains of a serine and histidine residue are suitably positioned to provide hydrogen bonding partners to the O4 carbonyl and methoxy groups of ubiquinone, respectively. This allows us to propose a mechanism for the reduction of ubiquinone during the catalytic turnover of the enzyme.

The Complex II family is comprised of two homologous integral membrane proteins (1–4). Succinate:quinone oxidoreductase (SQR),[4] or succinate dehydrogenase (SDH), is a functional member of the Krebs cycle and the aerobic respiratory chain coupling the oxidation of succinate to fumarate with the reduction of quinone (Q) to quinol (QH_2). Quinol:fumarate oxidoreductase (QFR), or fumarate reductase, catalyzes the reverse reaction to SQR during anaerobic respiration. Both enzymes have a similar subunit and cofactor composition (1–4). The hydrophilic subunits, composed of a flavoprotein (SdhA) and an iron-sulfur protein (SdhB), have a high degree of sequence homology across species. The SdhAB catalytic subunits are anchored to the membrane by the hydrophobic SdhCD subunits, which in the case of mammalian and *Escherichia coli* Complex II form a cytochrome *b* that contains one heme *b*. The two-electron oxidation of succinate at the substrate binding site in the SdhA subunit is coupled to the two-electron reduction of quinone in the membrane domain of Complex II. Electrons are sequentially transferred to ubiquinone (in the case of mammalian and *E. coli* Complex II) via an electron transport chain consisting of a covalently bound flavin adenine dinucleotide (FAD) and three iron-sulfur centers ([2Fe-2S], [4Fe-4S], and [3Fe-4S]). The structures of SQRs and QFRs have been solved (5–8) revealing differences in the nature of quinone binding between SQR and QFR.

Quinones can undergo $2e^-/2H^+$ oxidation-reduction reactions, an essential feature of respiration, allowing the transfer of electrons between the respiratory complexes via the membrane-bound quinone pool. The high resolution crystal structures of a number of quinone-reactive membrane proteins have revealed their quinone-binding sites (Q-sites) and facilitated their detailed analysis. These structures and contributions from biochemical, mutagenic, inhibitor binding, EPR, and Fourier transform infrared studies have highlighted significant variation, and at times controversy, in the mechanisms and architecture of quinone binding. A weak sequence motif associated with the presence of a Q-site has been proposed (9); however, currently no common architecture or universal catalytic mechanism can be applied to Q-sites in general. In addition to this, significant variability is seen for quinone binding in the same protein from different species, as for example in the bc_1 complex (10, 11). Different redox states of quinones may also adopt different conformations in the quinone-binding pockets as has been shown for the photosynthetic bacterial reaction center (12). In the case

* This work was supported by the Biotechnology and Biological Sciences Research Council (to R. H. and S. I.), by Syngenta (to R. H., S. I., G. S., and W. W.), and by National Institutes of Health Grant GM61606 and the Dept. of Veterans Affairs (to G. C.). The costs of publication of this article were defrayed in part by the payment of page charges. This article must therefore be hereby marked "*advertisement*" in accordance with 18 U.S.C. Section 1734 solely to indicate this fact.

The atomic coordinates and structure factors (code 2ACZ) have been deposited in the Protein Data Bank, Research Collaboratory for Structural Bioinformatics, Rutgers University, New Brunswick, NJ (http://www.rcsb.org/).

[1] Current address: Chalmers University of Technology, Lundberg Laboratory, Medicinaregatan 9E, SE-41390 Gothenburg, Sweden.

[2] To whom correspondence may be addressed: Molecular Biology (151-S), Veterans Affairs Medical Center, San Francisco, CA 94121. Tel.: 415-221-4810 (ext. 4416); Fax: 415-750-6959; E-mail: ceccini@itsa.ucsf.edu.

[3] To whom correspondence may be addressed: Division of Molecular Biosciences, Imperial College London, London SW7 2AZ, United Kingdom. Tel.: 44-2075-943064; Fax: 44-2075-943022; E-mail: s.iwata@imperial.ac.uk.

[4] The abbreviations used are: SQR, succinate:ubiquinone oxidoreductase; QFR, menaquinol:fumarate oxidoreductase; AA5, atpenin A5; SDH, succinate dehydrogenase; DNP17, 2-(1-methylhexyl)-4,6-dinitrophenol; Q, quinone; QH_2, quinol.

TABLE 1
Summary of the chemical structures and properties of some well characterized ubiquinone analogues and Complex II Q-site inhibitors

Name	Abbreviation	Chemical name	Chemical structure	No. of rotatable bonds	Reference
Ubiquinone-2	Q2	2,3-dimethoxy-5-geranyl-6-methyl-1,4-benzoquinone	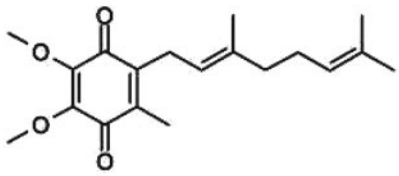	13	36
Atpenin A5	AA5	3-[(2S,4S,5R)-5,6-dichloro-2,4-dimethyl-1-oxohexyl]-4-hydroxy-5,6-dimethoxy-2(1H)-pyridinone	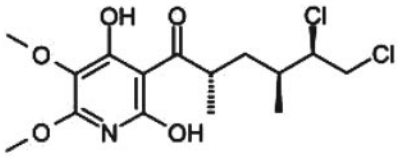	14	24, 25
Dinitrophenol -17	DNP17	2-(1-methylhexyl)-4,6-dinitrophenol	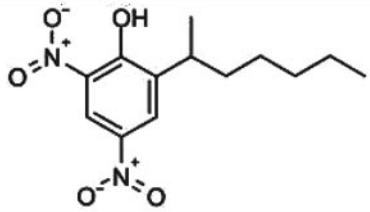	7	44
Carboxin	Cbx	5,6-dihydro-2-methyl-1,4-oxathiin-3-carboxanilide	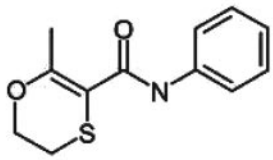	3	20, 21
2-Thenoyltri-fluoroacetone	TTFA	4,4,4-trifluoro-1-(2-thienyl)-1,3-butanedione	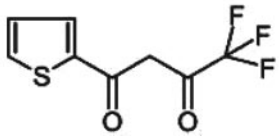	4	20, 22, 23

of Complex II, a ubiquinone-binding site was found in SQR proximal to the [3Fe-4S] cluster (7, 8). In *E. coli* QFR, one functional menaquinone site is also found proximal to the [3Fe-4S] cluster (13), but its location and residue composition are very different to that of *E. coli* SQR. In addition, a second menaquinone-binding site, apparently not participating in electron transfer, is found on the distal side of the membrane (5) at a position similar to a weak inhibitor-binding site in mammalian SQR (8). The *Wolinella succinogenes* QFR site for menaquinol oxidation has not yet been observed structurally (6), however, mutagenic and kinetic data suggest that the site is located distal from the [3Fe-4S] cluster (14).

The single *E. coli* SQR Q-site is homologous to that of mammalian SQR based on the absolute conservation of amino acids in contact with ubiquinone (7, 8) suggesting the same mechanism for electron transfer to ubiquinone thus making it an excellent model system for mitochondrial Complex II research. This is of particular interest in humans, because mutations in Complex II results in various physiological disorders, including paraganglioma and pheochromocytoma tumors (15–17). Indeed, the nuclear *SdhB*, *SdhC*, and *SdhD* genes encoding Complex II are classed as tumor suppressor genes. Furthermore, in *Caenorhabditis elegans* the SdhC Gly-71 → Glu mutation (*mev-1*) causes premature aging resulting in a reduced life span and increased production of reactive oxygen species (18). A similar effect has also been seen in a mouse model (19). The structure of SQR from *E. coli* (7) shows that the equivalent residues to those mutated in the paraganglioma and *mev-1* phenotypes are located at the Q-site and may perturb quinone binding and/or reduction. A detailed understanding of the Q-site in Complex II and mechanism of quinone binding and reduction could assist the development of suitable treatments for these human disease states.

In this work, we present the crystallographic and computational analysis of the Q-site of *E. coli* SQR using a specific and potent inhibitor, also known to be effective in mammalian Complex II. Previously, carboxin (20, 21) and thenoyltrifluoroacetone (20, 22, 23) had been used for the analysis of the Q-site of Complex II. More recently a new specific Q-site inhibitor for Complex II, Atpenin A5 (AA5), was reported and characterized (24, 25). SQR from *E. coli* is strongly inhibited by AA5 making it an excellent tool for the elucidation of the characteristics of the Com-

plex II Q-site. Table 1 summarizes the structure and properties of some well characterized ubiquinone analogues and Complex II Q-site inhibitors.

In the *E. coli* SQR structure (7) a tyrosine residue (Tyr-83) is proposed to be the primary ligand for ubiquinone; a binding position referred to here as the Q_1-site. A tyrosine residue ligating quinone is a unique feature to SQR. However, new evidence, presented by this work, suggests that other residues located at the Q-site in Complex II could be directly involved in ubiquinone ligation and reduction during catalysis. The Q-site of *E. coli* SQR has been analyzed in detail using a combination of x-ray crystallography and computational chemistry to reveal that ubiquinone reduction may occur deeper within the Q-site than previously proposed (7), at a position referred to here as the Q_2-site. These studies suggest a mechanism for the reduction of ubiquinone during the catalytic turnover of this interesting respiratory enzyme.

EXPERIMENTAL PROCEDURES

Expression, Purification, and Crystallization—These methods are as previously described (26, 27) with only minor modifications to the sample preparation following purification to introduce the inhibitor. Protein sample, containing ~60 mg ml^{-1} of purified SQR in Buffer C (20 mM Tris-HCl, 0.05% Thesit, pH 7.6) was diluted 1:10 with Buffer C plus 50 μM Atpenin A5 (AA5) and incubated at 4 °C for 14 h. Excess inhibitor was washed out by diluting (1:10) and re-concentrating the sample with Buffer C three times. The enzyme was then re-concentrated to ~60 mg ml^{-1} and used to set up crystallization trials by the hanging-drop vapor-diffusion method as previously described (27).

Data Collection and Structure Determination—Crystals were frozen within 72 h of a trial set up for x-ray data collection. The crystals were soaked in cryo-protectant containing the crystallization condition reagents plus 30% polyethylene glycol 400. Diffraction data were collected at −170 °C to 3.0 Å resolution using an Area Detector Systems Corporation detector on beam line ID29 at the European Synchrotron Radiation Facility, France. The x-ray diffraction from the crystals was anisotropic; there were reflections to 3.0 Å along the *c* axis, however, reflections beyond 3.5 Å resolution on the *a* and *b* axis plane were weak. Image data were processed to a resolution of 3.1 Å using the program packages DENZO and SCALEPACK (28). All data better than -2.0σ(I) were used for scaling. The crystals belong to the trigonal space group *R*32 with cell dimensions of $a = b =$ 138.75 Å, $c = 521.87$ Å and one molecule per asymmetric unit, very similar to those previously obtained (27). Phase information was obtained from the native SQR structure (Protein Data Bank (PDB) 1NEK). A starting model for refinement was obtained by docking the AA5 inhibitor into the native structure with ubiquinone removed (PDB 1NEK less Q) using GOLD (31). The GOLD solutions were screened manually, one selected based on its fitness score, and that closely fitted the unrefined electron density and then its coordinates (see Fig. 2*B*) were combined with the native structure (PDB 1NEK less Q) to give the starting model. The program suite CNS (29) was used to solve and refine the structure, and the model was edited using the program O (30). The final R_{cryst} and R_{free} values were 26 and 30%, respectively, at 3.1 Å resolution, data collection and refinement statistics are summarized in Table 2, and the coordinates are available from the PDB data base (PDB code 2ACZ).

GOLD Setup—Protein coordinates (PDB 1NEK) were prepared using the program Sybyl 6.7 (www.tripos.com). A 14 Å sphere of the protein structure containing the Q-site at the center was selected, and ubiquinone (Q) was removed. Hydrogens were added, and lone pairs were removed with the final format as .mol2. Prior to protein-ligand docking using the program GOLD 1.2 (31) several preparative steps were taken. The center of the Q-site was identified ($x = 6.9$, $y = 4.9$, and $z = -24.4$) and applied to docking calculations. Initially, the default input files and options of GOLD were used. Initial docking experiments were hindered by the program's persistence in docking the hydrophobic tail of the ligand into the Q-site instead of the reactive head group. This is due to the lack of a hydrophobic environment outside of the protein *in silico* (normally within the membrane *in vivo*). The favorable hydrophobic interactions file (fit_pts.mol2) was customized using Sybyl; the position and hydrophobic environment of the membrane was mimicked by adding additional dummy atoms outside the protein/Q-site to create a virtual membrane.

Ligand Docking—An exhaustive docking approach was employed to identify all possible docking modes for each ligand, as described for the validation of GOLD (31). Each docking solution was scored using the "goldscore" function and then screened manually (by eye) using Sybyl. Unreasonable solutions such as where the hydrophobic tail of ubiquinone docked where the quinone headgroup should be found were discarded; the remainders were grouped based on similarity, and several examples were selected for further analysis. The protein-ligand interactions were verified using the "Ligand Protein Contacts" online server (32). The coordinates for the carboxin docking result (PDB 1NEK plus docked carboxin) is available from the PDB data base (PDB code 2AD0).

Figure Preparation—Coordinate files associated with GOLD (.mol2 format) were converted to PDB format using the program Vega Open GL 1.5.1 (33). All structure figures were prepared using PyMOL 0.98.[5] The sequence alignment was made using the T-Coffee online server (35) and edited using GeneDoc.[6]

RESULTS

Analysis of the SQR-AA5 co-complex structure (PDB 2ACZ) reveals that the protein is essentially unchanged from the native SQR structure (PDB 1NEK) with the exception that the inhibitor replaces ubiquinone at the Q-site. In the native structure the side chains of Tyr-D83 and Trp-B164 are direct ligands of the O1 atom of ubiquinone (7). There is, however, no amino acid side chain within proximity to the O4 carbonyl oxygen of the ubiquinone molecule in the native structure (Fig. 1*A*). Tyr-D83 forms an additional hydrogen bond to Arg-C31, and the Arg-C31 side chain is within 4 Å of the methoxy group of ubiquinone. The structure of SQR co-crystallized with 2-(1-methylhexyl)-4,6-dinitrophenol (DNP17, PDB 1NEN), a competitive inhibitor of SQR, binds at essentially the same position as ubiquinone in the native structure Fig. 1*B* (7). By comparison to ubiquinone in the native structure (Fig. 1*A*), this study shows that AA5 binds deeper into the Q-site. The binding site of AA5, named the Q_2-site (Fig. 2*A*), is at a very similar position to that suggested by the protein-ligand docking program GOLD when AA5 was docked into the native structure (Fig. 2*B*). Closer inspection of the protein environment at the Q_2-site reveals that Ser-C27 is positioned such that it can hydrogen bond with the N4 and O5 atoms of AA5 (Fig. 2*A*), whereas the O1 interactions remain the same as for ubiquinone at the Q_1-site in the native structure (Tyr-D83, Fig. 1*A*). In addition, these data are consistent with the fact that Ser-C27 is strictly conserved, as shown by the alignment of the SdhC sequences from a range of species (Fig. 3).

Interestingly, the position of AA5 at the Q_2-site is also in close proximity to His-B207, which is the furthest point from the opening of the Q-site. In the native structure (7), the $N\tau$ atom of His-B207 was hydrogen-bonded to a heme *b* propionate based on the presence of strong

[5] W. L. DeLano (2002) *The PyMOL Molecular Graphics System*, DeLano Scientific, San Carlos, CA (www.pymol.org).

[6] K. B. Nicholas, H. B. Nicholas, and D. W. Deerfield (1997) *EMBNEW News* **4,** 14 (www.psc.edu/biomed/genedoc).

TABLE 2
Data collection and refinement statistics for SQR-AA5 structure

Data collection and phasing	
Beamline	ESRF ID29
Wavelength (Å)	0.9393
Resolution (Å)	40.0–3.1
Total observations	148,726
Unique reflections	38,077
Completeness (%)[a]	97.5 (94.2)
Redundancy	4.36
I/σ(I)	14.7 (2.0)
R_{sym} (%)[a,b]	7.8 (33.7[c])
Refinement[d]	
Resolution (Å)[a]	40.0–3.1 (3.16–3.10)
R-factor (%)[a,e]	26.4 (37.6[c])
R_{free} (%)[a,f]	30.8 (42.9[c])
Average B values (Å^2)	73.7
Root mean square deviations from ideal values	
Bond length (Å)/angles (°)	0.0095/1.56
Ramachandran plot (non-Gly, non-Pro residues)	
Most favored regions (%)	80.2
Additional allowed regions (%)	17.6
Generously allowed regions (%)	1.9
Disallowed regions (%)	0.3

[a] Values in parentheses are for the highest resolution shell.
[b] $R_{sym} = \Sigma_h\Sigma_i|I_i(h) - \langle I(h)\rangle|/\Sigma_h\Sigma_i I(h)$, where $I_i(h)$ is the *i*th measurement.
[c] The last shell R_{merge} for the data set is high due to strong anisotropy. However, it is included to 3.1 Å in the refinement, because the *R*-factor and R_{free} for the shell are reasonably low, which indicates the data in this shell are still useful for the refinement.
[d] All the observed reflections are used for the refinement.
[e] $R\text{-factor} = \Sigma_h||F(h)_{obs}| - |F(h)_{calc}||/\Sigma_h|F(h)_{obs}|$.
[f] R_{free} was calculated for 1% of reflections randomly excluded from the refinement.

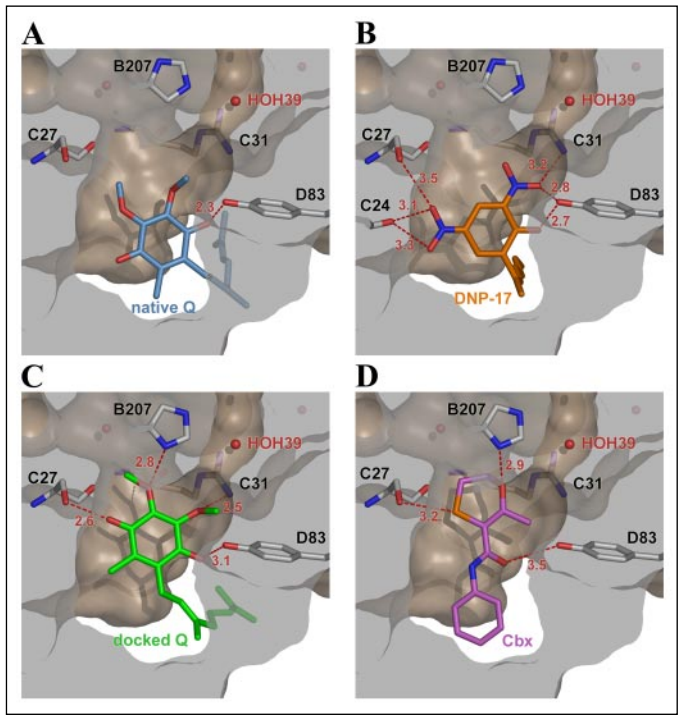

FIGURE 1. **Q-site in *E. coli* SQR; slab view with the surface and interior of the protein shown in beige and gray, respectively.** Binding positions at the Q_1-site for ubiquinone in the native structure (*blue*, PDB 1NEK) (*A*) and DNP17 inhibitor (*orange*, PDB 1NEN) (*B*) and the Q_2-site for GOLD docked ubiquinone (*green*) (*C*) and carboxin inhibitor (*Cbx*, *purple*, PDB 2AD0) (*D*). Key residues (*gray*) are labeled, and protein-ligand interactions shown by *red dotted lines* with the distances labeled.

electron density between the two atoms. To an extent, this is still the case when AA5 is bound at the site, but some additional electron density bridges the O3 atom of an AA5 methoxy group and His-B207 (~2.8 Å) (Fig. 2*A*). Along with the spherical shape of the electron density for the side chain of this residue, this suggests that the histidine may exhibit multiple conformations in the crystal structures and probably during catalysis; the $N\tau$ atom could interact with the AA5 methoxy group by a 180° rotation. This histidine residue is adjacent to Cys-B206, one of the ligands for the [3Fe-4S] cluster, which as a consequence positions it approximately equidistant between the three reduction centers: the [3Fe-4S] cluster, heme *b*, and the Q_2-site.

The proposal that a water molecule may act as the second ligand for ubiquinone (7) was investigated using the program SuperStar (37) (data not shown). The program revealed several possible water binding sites in the empty Q-site. However, repeating this experiment with ubiquinone bound at the Q_1-site, as found in the native structure (1NEK), resulted in the prediction of no water-binding sites. To date, there is no experimental evidence to support the hypothesis that water may be involved or that there is indeed a ligand for the O4 atom of ubiquinone at the Q_1-site in the native structure.

The protein-ligand docking program GOLD (31) was used to confirm the binding position of ubiquinone to the Q_1-site, as observed in the native structure (Fig. 1*A*). A range of inhibitors (Table 1) was also docked for comparison purposes. Varying lengths of the isoprene tail of ubiquinone were docked initially, but Q2 (ubiquinone-2, Table 1) with two isoprene units was selected for exhaustive docking experiments for several reasons. First, only two isoprene units of ubiquinone could be modeled in the native SQR structure (7) and second, in the photosynthetic reaction center the majority of the contribution to binding strength for quinones is contributed by the first two isoprene units (38). Several docking components (overall fitness, external hydrogen bonding, and external Van der Waals) were used by GOLD to score the ligands. Unexpectedly, GOLD consistently docked ubiquinone deeper into the Q-site at the same position at which AA5 was located (the Q_2-site) in the SQR-AA5 structure (Fig. 1*C*). Similarly, GOLD docked ubiquinol (QH_2) and other quinone intermediates at the same Q_2-site (data not shown).

The agreement between the SQR-AA5 structure and GOLD docking for AA5 demonstrated the reliability of protein-ligand docking using GOLD. Thus, the dockings for carboxin were analyzed in detail (Fig. 2*C*). Carboxin has considerably fewer rotatable bonds than ubiquinone or AA5 (Table 1), and consequently fewer possible modes (poses) of binding were suggested by GOLD. The dockings were classified into two modes of which 75% of the docking solutions were "Mode 1," 24% were "Mode 2," and one was an outlier from a total population of 100 solutions, Fig. 2*C*. Having only two modes, *i.e.* fewer possible correct answers, aided the selection of the final docking solution; the selected model is shown in Fig. 1*D*. This theoretical structure (PDB 2AD0) provides a useful model for carboxin inhibition, which is consistent with data on Complex II mutations (39). The docking suggests that the O7 atom of carboxin is only 2.9 Å from His-B207 (Fig. 1*D*). Mutation of His-B207 is known to result in carboxin resistance in a fungal model system (39). As suggested for the SQR-AA5 structure, this residue may exhibit multiple conformations during catalysis, and the $N\tau$ atom could interact directly with carboxin by a 180° rotation.

Further analysis of the native structure (PDB 1NEK) revealed a putative proton pathway suitable for the delivery of protons to the Q-site, which had not previously been described (7). The funnel-shaped opening of the pathway to the cytoplasm, located at the surface of the membrane, contains six water molecules (HOH1, -28, -49, -58, -76, and -113) (Fig. 4, *A* and *B*). This opening is linked to the Q-site, on the opposite side of the membrane anchor, by six additional waters (HOH24, -40, -51, -92, -99, and -115) and three ionizable side chains (Glu-C101, Asp-C95, and Lys-B230) (Fig. 4, *B* and *C*). The final water molecule in the

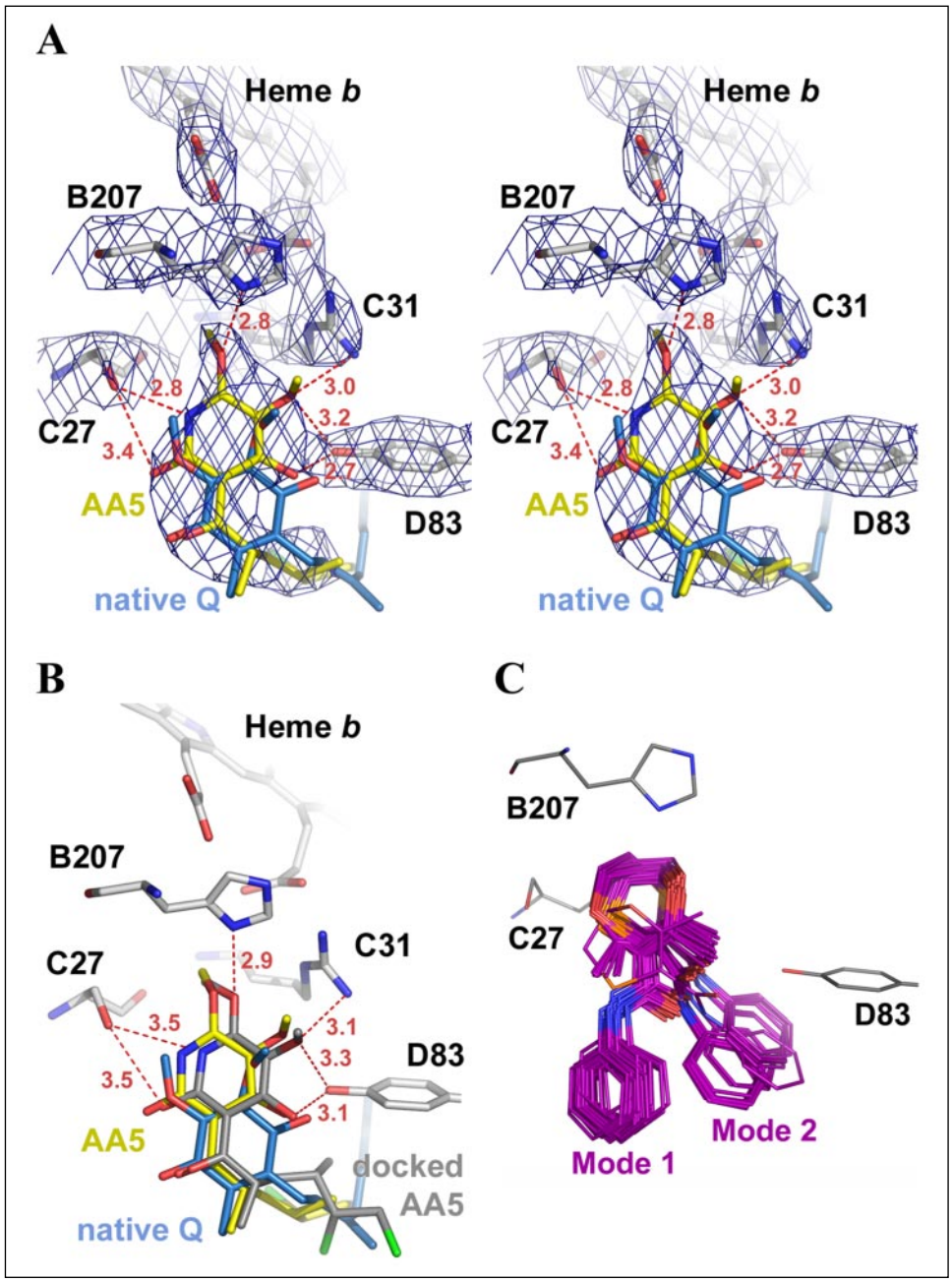

FIGURE 2. **Q_1-site (ubiquinone) and Q_2-site (AA5 and carboxin) comparison in *E. coli* SQR.** *A*, *stereo view* of SQR-AA5 crystal structure (*yellow*, PDB 2ACZ) compared with ubiquinone binding in the native SQR crystal structure (*blue*, PDB 1NEK) with $2F_o - F_c$ electron density map for the SQR-AA5 crystal structure after refinement contoured at 1.1σ. *B*, AA5 GOLD docking solution (*gray*) overlaid on the native SQR (*blue*) and SQR-AA5 crystal structure (*yellow*). This docking solution was used as the starting model for refinement of the SQR-AA5 crystal structure. *C*, all carboxin docking solutions superimposed (one hundred in total) showing the two modes of possible binding; 75% were *Mode 1*, 24% were *Mode 2*, and one outlier. The final docking solution selected from these is shown in Fig. 1*D* (PDB 2AD0). Key residues (*gray*) are labeled, and protein-ligand interactions shown by *red dotted lines* and the distances labeled.

pathway (HOH39) is coordinated by His-B207, Arg-C31, and Asp-D82 at the back of the Q_2-site (Fig. 4*C*). The average *B* value for the water molecules in the pathway is 43.2 Å^2, which is lower than the overall average *B* value for all the atoms in the native structure, 45.0 Å^2, suggesting these water molecules are highly ordered and reliably positioned.

DISCUSSION

In the native 2.6 Å resolution structure (7), ubiquinone is located at the fringe of a hydrophobic pocket (Fig. 1*A*) comprised of residues from three subunits; SdhB, SdhC, and SdhD. At this position, referred to as the Q_1-site, the side chain of Tyr-D83 (and Trp-B164) is in close proximity to the O1 carbonyl group of ubiquinone. The only continuous electron density between the protein environment and ubiquinone was from Tyr-D83 to the O1 atom of ubiquinone (7) suggesting this residue is the ligand for the O1 carbonyl of ubiquinone. In contrast, there were no suitable ligands in close proximity to the O4 atom of ubiquinone (Fig. 1*A*). Ligation of the O4 atom is a common feature of other structurally characterized Q-sites of respiratory proteins (9, 40–43). The lack of a ligand for the O4 carbonyl of ubiquinone resulted in the proposal that a water molecule could be involved (7), as found in the bc_1 complex (10, 11) and the anaerobic respiratory complex formate dehydrogenase (41). However, no water molecules were identified in the native structure of SQR, which was substantiated using the program SuperStar.

The Complex II inhibitor DNP17 (Table 1) (44) was previously co-crystallized with SQR (Fig. 1*B*) to confirm the location of the Q-site in SQR (7). DNP17 was found at the same position as ubiquinone in the native structure, the Q_1-site. In contrast to the native SQR and SQR-DNP17 structures, however, as shown in this work the SQR structure with AA5 bound reveals an alternative deeper binding position at the Q-site, named the Q_2-site (Fig. 2*A*). The position of AA5 at the Q_2-site in the crystal structure is in agreement with a protein-ligand docking

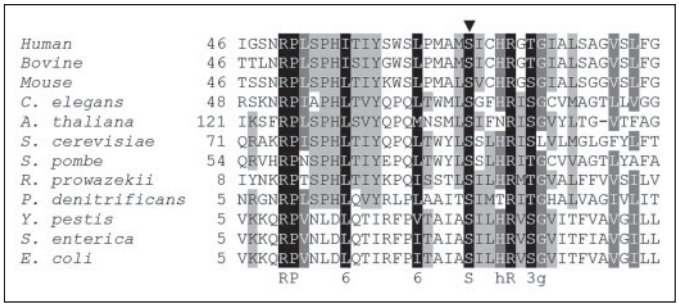

FIGURE 3. **SdhC sequence alignment from a range of species.** Residues that are 100%, 80%, and 60% conserved are highlighted in *black*, *dark gray*, and *light gray*, respectively. The conserved serine C27 is indicated by an *arrow* (▼). (Sequence alignment was made using T-Coffee (35) and viewed and edited using GeneDoc.[6])

solution obtained using the program GOLD, which suggested an almost identical position and orientation (Fig. 2*B*).

Interestingly, the program GOLD suggested that ubiquinone also bound at the Q_2-site similarly to AA5 (Fig. 1*C*). This result suggests that ubiquinone in SQR can adopt alternative conformations in the Q-binding pocket. While the O1 carbonyl atoms of both AA5 and the docked ubiquinone hydrogen bond with Tyr-D83 (2.7 and 3.1 Å respectively) in the same way as ubiquinone in the native SQR structure, they form additional interactions with the protein environment at the Q_2-site that are not possible when bound at the Q_1-site. The O5 and N4 atoms of AA5 (Fig. 2*A*) and the O4 carbonyl of the docked ubiquinone (Fig. 1*C*) are both in close proximity of Ser-C27 (3.4, 2.8, and 2.6 Å, respectively) and His-B207 (2.8 Å for both). Both residues have properties that suggest key roles in ubiquinone binding and reduction. Ser-C27 is strictly conserved throughout all species (Fig. 3). In addition, Yang and colleagues (45) also found that mutating this residue to alanine, cysteine, or threonine in *E. coli* SQR rendered the cells unable to grow on succinate, and the K_m for ubiquinone was undetectable. Interestingly, they also found that the association between the photoaffinity-labeled [3H]azido-Q and the SdhC subunit was lost in the Ser-C27 mutants suggesting a direct effect on quinone binding. In the case of His-B207, Broomfield *et al.* (39) showed that mutation of this histidine to a leucine in *Ustilago maydis* SQR, at the equivalent position to *E. coli* SQR, resulted in resistance to the Complex II-specific inhibitor carboxin (39, 46). The same result was also observed for *Paracoccus denitrificans* SQR (21).

The use of Ser-C27 as a hydrogen bonding partner for the O4 of ubiquinone would be an attractive scenario, because ligation of the O4 atom would greatly increase the stability of the semiquinone intermediate generated during catalytic reduction. A similar proposal has also so been made for *Saccharomyces cerevisiae* SQR based on a theoretical model generated from the other Complex II x-ray structures (47). In the bacterial photosynthetic reaction center, serine L223 is hydrogen-bonded to Q_B and has been proposed to be involved in proton-transfer events (12, 48, 49). It has been suggested that this hydrogen bond to the carbonyl oxygen of Q_B does not form when Q_B is in the neutral charge state (Q_B^0), but only in the reduced state (Q_{B-}) and is effected by the protonation state of a nearby acidic residue (Asp-L213). The presence of a nearby positive charge from Arg L217 may also considerably stabilize the hydrogen bond of the serine residue with the quinone (50). The presence or absence of this hydrogen bond has been speculated to be involved in the conformational gating for the electron transfer process from Q_A to Q_B (50). In addition, a serine residue has also been implicated as a hydrogen bond donor to the semiquinone at the Q_i site of the bc_1 complex (51, 52), which helps provide binding stability for the semiquinone.

Similarly, at the Q_2-site, His-B207 of SQR could provide additional

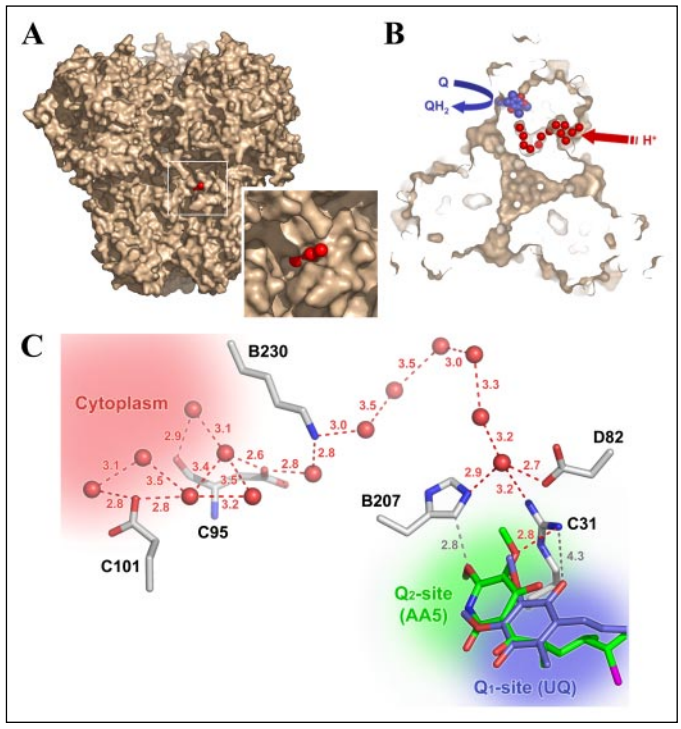

FIGURE 4. **Putative proton transfer pathway in *E. coli* SQR.** *A*, surface representation of the trimer with the opening of the pathway to the cytoplasm viewed parallel to the membrane and *B*, slab view from the cytoplasm along the membrane normal showing the path of the chain from one side of the anchor monomer to the Q-site on the other. The surface of the protein (*beige*), water molecules (*red space-fill*), and ubiquinone (*blue space-fill*) are shown. *C*, detailed view of the pathway from the cytoplasm (*red*) to the Q-site (*blue/green*) in *E. coli* SQR; water molecules (*red space-fill*) and conserved residue side chains (*gray*) interacting with the pathway are shown. Ubiquinone (Q_1-site, *blue*) and AA5 (Q_2-site, *green*) at the Q-site are labeled accordingly. Hydrogen bonds and other distances are shown by *red* and *gray dotted lines*, respectively, and the distances are labeled.

stability to the semiquinone intermediate generated during catalytic reduction by hydrogen bond formation between its $N\tau$ atom and one of the methoxy groups of ubiquinone. It is possible that the potency of inhibitors such as AA5 and carboxin is due to strong interactions with both Ser-C27 and His-B207, blocking ubiquinone from accessing the Q-site. Indeed, carboxin was docked into the SQR structure in the same way as ubiquinone and AA5 using the program GOLD to reveal that the inhibitor was in close proximity to the His-B207 as well as Ser-C27 and Tyr-D83 (Figs. 1*D* and 2*C*). Although no experimental structural data is available yet to confirm this docking result, these data along with the available mutation data (39) suggest that carboxin also binds at the Q_2-site. The agreement between the biochemical, genetic, and structural evidence for both residues point to a pivotal role in ubiquinone binding and reduction, and substantiating the hypothesis that ubiquinone reduction may occur at the Q_2-site.

To fully reduce the quinone in SQR, two protons and the two electrons from the oxidation of succinate are needed. This would require two protons to be donated to ubiquinone by the protein environment of the Q-site followed by re-protonation of the site after catalytic turnover. As part of this study, a proton uptake pathway was identified in the native structure (PDB 1NEK) suitable for such a purpose. The proton pathway crosses the membrane anchor (Fig. 4*B*) arriving at the Q-site between His-B207, Arg-C31, and Asp-D82 (Fig. 4*C*). At the Q_2-site the semiquinone species could be protonated by protons delivered to the Q-site via the last water molecule in the proton pathway (HOH39); the close proximity of His-B207 and Asp-D82 to HOH39 may also facilitate this process. Additional support for the validity of the proton transfer

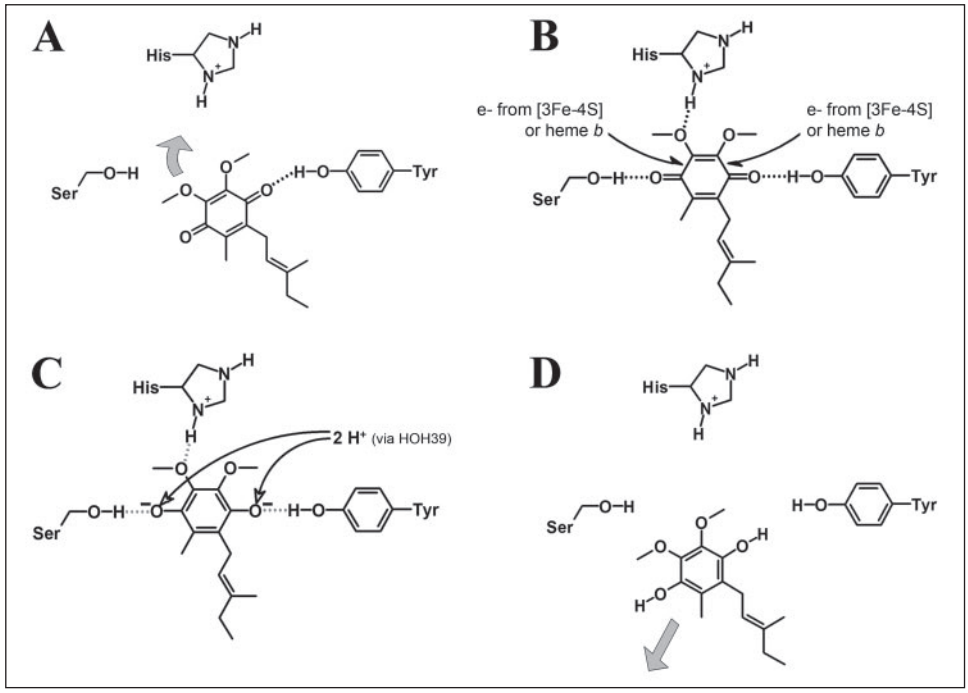

FIGURE 5. **Proposed Q-site reaction mechanism.** *A*, initially, ubiquinone binds at the opening of the Q-site, the Q_1-site, prior to catalytic reduction via a hydrogen bond between Tyr-D83 and the O1 carbonyl atom. The presence of electrons in the redox cofactor chain induces the movement of ubiquinone into the Q_2-site (*thick gray arrow*). This may involve alteration in the side-chain conformation of His-B207 in response to the redox status of the nearby [3Fe-4S] cluster. *B*, at the Q_2-site, hydrogen bond formation occurs from Ser-C27 and His-B207 to the O4 carbonyl and O3 methoxy groups of ubiquinone, respectively (*black dotted lines*). This allows the sequential delivery of two electrons to ubiquinone from either the [3Fe-4S] cluster and/or heme *b*. *C*, the phenolate dianion species formed when the two electrons arrive (*B*) is then doubly protonated via HOH39 and the proton transfer pathway, which coincides precisely with the disruption of the hydrogen bond stabilization of ubiquinone by Tyr-D83, Ser-C27, and His-B207 (*gray dotted lines*). *D*, the disruption of the hydrogen bond network allows the fully reduced ubiquinol molecule to leave the Q-site (*thick gray arrow*). The side chains of key residues are labeled accordingly with associated hydrogens shown where relevant. Hydrogen bonds are shown by *dotted lines*. Electron and proton movement is shown by *half-black* and *full-white curly arrows*, respectively.

pathway is found in the conservation of the residues interacting with the pathway; Lys-B230, Asp-C95, and Glu-C101 all bridge water molecules in the pathway (Fig. 4*C*) and are strictly conserved (data not shown). Similarly, His-B207, Arg-C31, and Asp-D82 coordinate the final water molecule in the pathway (Fig. 4*C*) and are also all conserved in SQR. Interestingly, the equivalent residue to Lys-B230 in the *E. coli* QFR structure (Lys-B228) is within hydrogen bonding distance of menaquinone (PDB 1LOV) and was suggested to be a possible proton donor to menaquinone in that system (42, 53). Mutation of this residue in QFR results in a marked reduction of quinone reductase activity and a lowering of the [3Fe-4S] cluster redox potential in QFR.[7] Lys-B230 in SQR, as noted above, bridges water molecules in the hypothetical proton transfer pathway of SQR and is also in close proximity to the backbone carbonyl of Cys-B206, one of the ligands of the [3Fe-4S] cluster. If Lys-B230 in SQR affects the redox potential of the [3Fe-4S] cluster like Lys-B228 of QFR, this may suggest a redox-linked control of the protonation pathway to the Q-site of SQR. In the case of Asp-C95, work by Lemire and colleagues showed that mutation of the equivalent residue and region in *S. cerevisiae* SQR (Asp-C117) resulted in reduced enzyme activity (34) consistent with perturbation of the water pathway being important for protonation of the quinone in SQR.

The question remains as to why there is a 2.8 Å root mean squared deviation between the position of ubiquinone in the native structure (Q_1-site) and the position of ubiquinone when docked by the program GOLD (Q_2-site). Several hypotheses can be proposed to explain this difference. First, the Q_1-site could be an artifact of crystallization; some of the interactions between the endogenous ubiquinone (ubiquinone-8) and the protein environment may be diminished during crystallization and/or radiation with X-rays. This could facilitate the rotation of ubiquinone out of the Q-site around the Tyr-D83 hydrogen bond into a more "relaxed" conformation. Second, it is also possible that ubiquinone at the Q_1-site could be a reaction intermediate where ubiquinone could shift slightly out during catalytic turnover. Finally, a plausible explanation could be that ubiquinone binds weakly at the opening of the Q-site (Q_1-site) prior to catalytic reduction, because the enzyme has been crystallized in the oxidized form as evidenced by the binding of oxaloacetate at the substrate binding site in the SdhA subunit. During catalytic turnover of the enzyme, the presence of electrons in the redox cofactor chain, as a consequence of succinate oxidation at FAD, could induce the movement of ubiquinone from the Q_1-site into the Q_2-site to facilitate electron delivery and protonation via HOH39. This would be a logical solution, because ubiquinone waiting at the Q_1-site prior to catalytic reduction at the Q_2-site would negate quinone binding as a possible rate-limiting step.

Based on these findings, we have proposed a reaction mechanism for the reduction of ubiquinone at the Q-site in *E. coli* SQR (Fig. 5). Initially, ubiquinone binds at the opening of the Q-site, the Q_1-site, prior to catalytic reduction (Fig. 5*A*), consequently, quinone binding is not a rate-limiting step. The O1 carbonyl group of ubiquinone is orientated at this position by hydrogen bond interactions with Tyr-D83 and Trp-B164. The presence of electrons in the redox cofactor chain following the oxidation of succinate at FAD induces the movement of ubiquinone into the Q_2-site (Fig. 5*B*). This facilitates a second hydrogen bond interaction between the O4 carbonyl group of ubiquinone and Ser-C27. Additional stability of the binding of ubiquinone at the Q_2-site site could be provided by a hydrogen bond interaction between the O3 methoxy group of ubiquinone and His-B207. The orientation of the side chain of His-B207 may be determined by the redox status of the [3Fe-4S] center (and heme *b*), which may influence the occupancy of the Q_2-site by ubiquinone. When the Q_2-site is occupied by ubiquinone the $N\tau$ atom of His-B207 is oriented toward the methoxy group of the quinone, whereas when the site is unoccupied as in the native 1NEK crystal structure the orientation of His-B207 is different. The charge on His-B207 may also facilitate hydrogen bond formation between Ser-C27 and the quinone as proposed for the Q_B site of the reaction center (50). This suggests that His-B207 could play a gating function in electron transfer from the [3Fe-4S] cluster to the quinone and/or the heme *b* moiety of the enzyme, a potential mechanism by which the first electron is delivered to ubiquinone from either the [3Fe-4S] cluster or heme *b* (Fig. 5*B*). To limit the lifetime of the semiquinone radical, the second electron is

[7] E. Maklashina, R. Rothery, J. H. Weiner, and G. Cecchini, manuscript in preparation.

almost simultaneously delivered to ubiquinone from either the [3Fe-4S] cluster or heme *b* (Fig. 5*B*). Ubiquinone is then doubly protonated via HOH39 and the proton transfer pathway (Fig. 5*C*). This protonation event coincides precisely with the disruption of the hydrogen bond stabilization of ubiquinone by Tyr-D83, Ser-C27, and His-B207. The fully reduced ubiquinol molecule, which is expected to bind less tightly (12), can then leave the Q-site (Fig. 5*D*).

In summary, this work has identified a new binding position, the Q_2-site, at the Q-site of *E. coli* SQR. Evidence for this binding position is supported by the crystal structure of SQR with the inhibitor Atpenin A5 bound and protein-ligand docking data for ubiquinone. Several residues, identified by biochemical analysis as critical to the function of SQR, have clear structural and functional roles based on these observations. We have also described a proton pathway identified in the original native structure suitable for the delivery of protons to Q-site. Furthermore, from these data we have been able to propose a plausible reaction mechanism for ubiquinone reduction by Complex II. Additional experiments are in progress to substantiate these findings and further define the architecture of the Q-site of SQR.

Acknowledgments—We thank Susanna Törnroth-Horsefield, Richard Neutze, Tina Iverson, and Mika Jormakka for discussion and comments.

REFERENCES

1. Hägerhäll, C. (1997) *Biochim. Biophys. Acta* **1320,** 107–141
2. Cecchini, G., Schröder, I., Gunsalus, R. P., and Maklashina, E. (2002) *Biochim. Biophys. Acta* **1553,** 140–157
3. Lancaster, C. R. (2002) *Biochim. Biophys. Acta* **1553,** 1–6
4. Horsefield, R., Iwata, S., and Byrne, B. (2004) *Curr. Protein Pept. Sci.* **5,** 107–118
5. Iverson, T. M., Luna-Chavez, C., Cecchini, G., and Rees, D. C. (1999) *Science* **284,** 1961–1966
6. Lancaster, C. R., Kröger, A., Auer, M., and Michel, H. (1999) *Nature* **402,** 377–385
7. Yankovskaya, V., Horsefield, R., Törnroth, S., Luna-Chavez, C., Miyoshi, H., Léger, C., Byrne, B., Cecchini, G., and Iwata, S. (2003) *Science* **299,** 700–704
8. Sun. F., Huo, X., Zhai, Y., Wang, A., Xu, J., Su., Bartiam., and Rao, Z. (2005) *Cell* **121,** 1043–1057
9. Fisher, N., and Rich, P. R. (2000) *J. Mol. Biol.* **296,** 1153–1162
10. Hunte, C., Koepke, J., Lange, C., Rossmanith, T., and Michel, H. (2000) *Structure Fold Des.* **8,** 669–684
11. Berry, E. A., and Huang, L. S. (2003) *FEBS Lett.* **555,** 13–20
12. Stowell, M. H. B., McPhillips, T. M., Rees, D. C., Soltis, S. M., Abresch, E., and Feher, G. (1997) *Science* **276,** 812–816
13. Rothery, R. A., Seime, A. M., Spiers, A. M., Maklashina, E., Schroder, I., Gunsalus, R. P., Cecchini, G., and Weiner, J. H. (2005) *FEBS J.* **272,** 313–326
14. Lancaster, C. R., Gross, R., Haas, R., Ritter, M., Mantele, W., Simon, J., and Kröger, A. (2000) *Proc. Natl. Acad. Sci. U. S. A.* **97,** 13051–13056
15. Parfait, B., Chretien, D., Rotig, A., Marsac, C., Munnich, A., and Rustin, P. (2000) *Hum. Genet.* **106,** 236–243
16. Baysal, B. E., Rubinstein, W. S., and Taschner, P.E. (2001) *J. Mol. Med.* **79,** 495–503
17. Rustin, P., and Rötig, A. (2002) *Biochim. Biophys. Acta* **1553,** 117–122
18. Ishii, N., Fujii, M., Hartman, P. S., Tsuda, M., Yasuda, K., Senoo-Matsuda, N., Yanase, S., Ayusawa, D., and Suzuki, K. (1998) *Nature* **394,** 694–697
19. Ishii, T., Yasuda, K., Akatsuka, A., Hino, O., Hartman, P. S., and Ishii, N. (2005) *Cancer Res.* **65,** 203–209
20. Ramsay, R. R., Ackrell, B. A. C., Coles, C. J., Singer, T. P., White, G. A., and Thorn, G. D. (1981) *Proc. Natl. Acad. Sci. U. S. A.* **78,** 825–828
21. Matsson, M., and Hederstedt, L. (2001) *J. Bioenerg. Biomembr.* **33,** 99–105
22. Ingledew, W. J., and Ohnishi, T. (1977) *Biochem. J.* **164,** 617–620
23. Grivennikova, V. G., and Vinogradov, A. D. (1982) *Biochim. Biophys. Acta* **682,** 491–495
24. Ōmura, S., Tomoda, H., Kimura, K., Zhen, D.-Z., Kumagai, H., Igarashi, K., Imamura, N., Takahashi, Y., Tanaka, Y., and Iwai, Y. (1988) *J. Antibiot.* **41,** 1769–1773
25. Miyadera, N., Shiomi, K., Ui, H., Yamaguchi, Y., Masuma, R., Tomoda, H., Miyoshi, H., Osanai, A., Kita, K., and Ōmura, S. (2003) *Proc. Natl. Acad. Sci. U. S. A.* **100,** 473–477
26. Maklashina, E., Berthold, D. A., and Cecchini, G. (1998) *J. Bacteriol.* **180,** 5989–5996
27. Horsefield, R., Yankovskaya, V., Törnroth, S., Luna-Chavez, C., Stambouli, E., Barber, J., Byrne, B., Cecchini, G., and Iwata, S. (2003) *Acta Cryst.* **D59,** 600–602
28. Otwinowski, Z., and Minor, W. (1997) *Methods Enzymol.* **276,** 307–326
29. Brünger, A. T., Adams, P. D., Clore, G. M., DeLano, W. L., Gros, P., Grosse-Kunstleve, R. W., Jiang, J. S., Kuszewski, J., Nilges, M., Pannu, N. S., Read, R. J., Rice, L. M., Simonson, T., and Warren, G. L. (1998) *Acta Crystallogr. Sect. D* **54,** 905–921
30. Jones, T. A., Zou, J. Y., Cowan, S. W., and Kjeldgaard, M. (1991) *Acta Crystallogr. Sect. A* **47,** 110–119
31. Verdonk, M. L., Cole, J. C., Hartshorn, M. J., Murray, C. W., and Taylor, R. D. (2003) *Proteins* **52,** 609–623
32. Sobolev, V., Sorokine, A., Prilusky, J., Abola, E. E., and Edelman, M. (1999) *Bioinformatics* **15,** 327–332
33. Pedretti, A., Villa, L., and Vistoli, G. (2002) *J. Mol. Graph. Model* **21,** 47–49
34. Oyedotun, K. S., and Lemire, B. D. (1999) *J. Biol. Chem.* **274,** 23956–23962
35. Notredame, C., Higgins, D. G., and Heringa, J. (2000) *J. Mol. Biol.* **302,** 205–217
36. Crane, F. L., and Low, H. (1966) *Physiol. Rev.* **46,** 662–695
37. Verdonk, M. L., Cole, J. C., and Taylor, R. D. (1999) *J. Mol. Biol.* **289,** 1093–1108
38. Warncke, K., Gunner, M. R., Braun, B. S., Gu. L., Yu, C.-A., Bruce, M., and Dutton, P. L. *Biochemistry* **33,** 7830–7841
39. Broomfield, P. L., and Hargreaves, J. A. (1992) *Curr. Genet.* **22,** 117–121
40. Deisenhofer, J., Epp, O., Sinning, I., and Michel, H. (1995) *J. Mol. Biol.* **246,** 429–457
41. Jormakka, M., Törnroth, S., Byrne, B., and Iwata, S. (2002) *Science* **295,** 1863–1868
42. Iverson, T. M., Luna-Chavez, C., Croal, L., Cecchini, G., and Rees, D. C. (2002) *J. Biol. Chem.* **277,** 16124–16130
43. Ferreira, K. N., Iverson, T. M., Maghlaoui, K., Barber, J., and Iwata, S. (2004) *Science* **303,** 1831–1838
44. Yankovskaya, V., Sablin, S., Ramsay, R. R., Singer, T. P., Ackrell, B. A. C., Cecchini, G., and Miyoshi, H. (1996) *J. Biol. Chem.* **271,** 21020–21024
45. Yang, X., Yu, L., He, D., and Yu, C.-A. (1998) *J. Biol. Chem.* **273,** 31916–31923
46. Keon, J. P., Broomfield, P. L., White, G. A., and Hargreaves, J. A. (1994) *Biochem. Soc. Trans.* **22,** 234–237
47. Oyedotun, K. S., and Lemire, B. D. (2004) *J. Biol. Chem.* **279,** 9424–9431
48. Paddock, M. L., McPherson, P. H., Feher, G., and Okamura, M. Y. (1990) *Proc. Natl. Acad. Sci. U. S. A.* **87,** 6803–6807
49. Paddock, M. L., Feher, G., and Okamura, M. Y. (2003) *FEBS Lett.* **555,** 45–50
50. Ishikita, H., and Knapp, E.-W. (2004) *J. Am. Chem. Soc.* **126,** 8059–8064
51. Kolling, D. R. J., Samoilova, R. I., Holland, J. T., Berry, E. A., Dikanov, S. A., and Crofts, A. R. (2003) *J. Biol. Chem.* **278,** 39747–39754
52. Dikanov, S. A., Samoilova, R. I., Kolling, D. R. J., Holland, J. T., and Crofts, A. R. (2004) *J. Biol. Chem.* **279,** 15814–15823
53. Cecchini, G. (2003) *Annu. Rev. Biochem.* **72,** 77–109